Published in final edited form as:
Eur J Nucl Med Mol Imaging. 2014 December ; 41(12): 2337–2345. doi:10.1007/s00259-014-2856-x.

^{18}F-FDG PET of the hands with a dedicated high-resolution PEM system (arthro-PET): correlation with PET/CT, radiography and clinical parameters

Joyce C. Mhlanga,
Division of Nuclear Medicine, The Russell H. Morgan Department of Radiology and Radiological Sciences, Johns Hopkins University School of Medicine, Baltimore, MD, USA

John A. Carrino,
Division of Musculoskeletal Radiology, The Russell H. Morgan Department of Radiology and Radiological Sciences, Johns Hopkins University School of Medicine, Baltimore, MD, USA

Martin Lodge,
Division of Nuclear Medicine, The Russell H. Morgan Department of Radiology and Radiological Sciences, Johns Hopkins University School of Medicine, Baltimore, MD, USA

Hao Wang, and
Department of Oncology Biostatistics Division, Johns Hopkins University School of Medicine, Baltimore, MD, USA

Richard L. Wahl
Division of Nuclear Medicine, The Russell H. Morgan Department of Radiology and Radiological Sciences, Johns Hopkins University School of Medicine, Baltimore, MD, USA

Division of Nuclear Medicine, Johns Hopkins University Hospitals, 601 N. Caroline Street, JHOC 3233, Baltimore, MD 21287-0817, USA

Richard L. Wahl: rwahl@jhmi.edu

Abstract

Purpose—The aim of this study was to prospectively determine the feasibility and compare the novel use of a positron emission mammography (PEM) scanner with standard PET/CT for evaluating hand osteoarthritis (OA) with ^{18}F-FDG.

Methods—Institutional review board approval and written informed consent were obtained for this HIPAA-compliant prospective study in which 14 adults referred for oncological ^{18}F-FDG PET/CT underwent dedicated hand PET/CT followed by arthro-PET using the PEM device. Hand radiographs were obtained and scored for the presence and severity of OA. Summed qualitative and quantitative joint glycolytic scores for each modality were compared with the findings on plain radiography and clinical features.

Correspondence to: Richard L. Wahl, rwahl@jhmi.edu.

Parts of this paper were presented at the 2012 SNMMI meeting as an oral presentation.

Conflicts of interest None.

Results—Eight patients with clinical and/or radiographic evidence of OA comprised the OA group (mean age 73±7.7 years). Six patients served as the control group (53.7±9.3 years). Arthro-PET quantitative and qualitative joint glycolytic scores were highly correlated with PET/CT findings in the OA patients (r=0.86. p =0.007; r=0.94, p=0.001). Qualitative arthro-PET and PET/CT joint scores were significantly higher in the OA patients than in controls (38.7±6.6 vs. 32.2±0.4, p=0.02; 37.5±5.4 vs. 32.2±0.4, p=0.03, respectively). Quantitative arthro-PET and PET/CT maximum SUV-lean joint scores were higher in the OA patients, although they did not reach statistical significance (20.8±4.2 vs. 18±1.8, p= 0.13; 22.8±5.38 vs. 20.1±1.54, p=0.21). By definition, OA patients had higher radiographic joint scores than controls (30.9±31.3 vs. 0, p=0.03).

Conclusion—Hand imaging using a small field of view PEM system (arthro-PET) with FDG is feasible, performing comparably to PET/CT in assessing metabolic joint activity. Arthro-PET and PET/CT showed higher joint FDG uptake in OA. Further exploration of arthro-PET in arthritis management is warranted.

Keywords

PET/CT; Positron emission mammography (PEM); Osteoarthritis (OA); Arthritis; ^{18}F-Fluoro- 2-deoxy-D-glucose (FDG)

Introduction

Osteoarthritis (OA) is the most prevalent joint disorder in the elderly and is considered a chronic “degenerative” disease characterized by pain, local tissue damage and reparative phenomena. Cartilage damage was believed to be the sine qua non for OA. Since cartilage is an avascular, aneural tissue, the mechanisms of pain are expected to be influenced by other structures related to the articulation such the subchondral bone and soft tissue (e.g. synovium). Morphological imaging hall-marks of OA include loss of articular cartilage, osteophytes and a subarticular bone reaction (edema/sclerosis/cysts). Synovitis is increasingly recognized as an important feature of the pathophysiology of OA, although there is conflicting evidence with respect to its association with disease severity and clinical parameters [1]. Moreover, the presence of local joint inflammation, altered cartilage, and soft tissue and bone changes in OA implies a potential role for molecular mediators in OA pain [2]. This provides a reasonable target for functional imaging techniques such as nuclear medicine.

Imaging is considered essential for evaluating the variety of articulation-related structures for diagnosis, prognosis, and follow-up [3]. Radiography is typically the first-line imaging examination in a clinical setting when evaluating a patient with a known or suspected OA with limited sensitivity in the measurement of disease progression and weak-to-moderate correlation with clinical symptoms [4]. Contrast-enhanced MR imaging and ultrasonography are the most important methods for assessing synovitis associated with OA [5]. MRI is the standard for depicting synovitis in inflammatory arthritis, with increased contrast-enhanced uptake by the inflamed synovium due to hypervascularization and capillary permeability [6]. MRI is time-intensive and requires the administration of a gadolinium-based contrast agent which some patients cannot tolerate due to renal impairment or hypersensitivity. MRI may

be limited by patient claustrophobia or the presence of MRI-incompatible devices. Ultrasonography can depict synovial proliferation and joint effusions but is less sensitive than MRI in detecting bone erosions and marrow changes [7]. Ultrasonography is also operator-dependent and time-dependent with much variability in clinical practice. Irrespective of modality, a challenge that remains is interpreting the responsiveness of imaging techniques, in part due to lack of robust quantitative methods [8].

Nuclear medicine also offers new insights into the assessment of degenerative joint disease [9, 10]. ^{99m}Tc-Methyldiphosphonate (^{99m}Tc-MDP) bone scintigraphy can demonstrate increased joint tracer uptake in degenerative and inflammatory arthritis, although uptake can be seen in various conditions including trauma and infection [11, 12]. The role of ^{18}F-FDG PET in the diagnosis, staging, and monitoring of neoplastic conditions is well established. Animal data indicate that ^{18}F-fluoride PET is also potentially useful for the early detection of OA [13]. The clinical utility of using ^{18}F-FDG PET/CT is expanding to the diagnosis of nonneoplastic conditions that contain an inflammatory component, such as OA [14], because of its ability to depict hypermetabolism in these and other inflammatory joint conditions [15–26]. FDG accumulation in inflammatory conditions is likely secondary to the enhanced glycolytic metabolism in inflammatory cellular infiltrates including activated macrophages, neutrophils and lymphocytes [27]. Small field-of-view (FOV) positron emission mammography (PEM) systems designed for breast imaging have better spatial resolution than conventional larger FOV whole-body (WB) PET/CT systems [28]. Such systems are also less costly than WBPET systems. Thus, PEM systems appear potentially well suited to the imaging of inflammation in small synovial joints and may overcome some of the limitations of MRI and ultrasonography.

The aim of this study was to prospectively determine the feasibility and compare the novel use of a positron emission mammography (PEM) scanner with standard PET/CT for evaluating hand OA with ^{18}F-FDG.

Methods

Patient characteristics and study design

Institutional review board approval and written informed patient consent were obtained for this Health Insurance Portability and Accountability Act-compliant study. We prospectively identified 14 adult patients who were undergoing WB ^{18}F-FDG PET/CT for known or suspected cancer between March and July 2011. Inclusion criteria were: patient older than 21 years; patient agreement to additional hand imaging after a standard PET/CT scan; ability to lie prone for a 10-min dedicated hand PET/CT scan and have subsequent hand PEM imaging and radiography.

All patients completed an arthritis symptom questionnaire regarding the presence and type of arthritis (if known), treatment details, and history of joint swelling or deformity, pain, stiffness or restriction of activities. A focused clinical examination of the hand joints was performed by one of the investigators and joint deformity, swelling, warmth, redness and tenderness were assessed as per the American College of Rheumatology (ACR) OA classification [29]. These investigations were performed before the WB PET/CT scans.

Following acquisition of the clinical WB PET/CT examination, additional dedicated PET/CT imaging of the hands was performed, followed immediately by arthro-PET (PEM). Standardized two-view anterior/posterior and oblique digital radiographs of both hands were obtained (Fig. 1).

Acquisition of PET/CT images

Standard WB ^{18}F-FDG PET/CT scans were performed on a Discovery VCT (RX) system (GE Healthcare, Waukesha, WI) using standard clinical protocols [30]. All patients fasted for a minimum of 4 h and had serum glucose levels less than 200 mg/dL before intravenous injection of a weight-based amount of ^{18}F-FDG (0.22 mCi/kg, 8.14 MBq/kg). After a targeted 60-min tracer uptake phase, a combined WB PET/CT scan was performed. Extremity PET/CT images of the hands were then acquired with the patient lying in a prone position, hands raised above the head (Fig. 1). This involved an additional low-dose upper extremity CT scan of the hands and wrist for attenuation correction using a 64-slice multidetector helical scanner, followed by a 3-D PET emission scan. Dedicated hand emission PET scans were acquired over two bed positions, 4.3 min per bed position. The dedicated hand CT scan was acquired using 120 kVp and 40 mA, with a tube rotation time of 0.5 s, pitch of 0.984, and matrix size of 512 × 512 and 0.977 × 0.977 × 3.27 mm voxels. The PET images were reconstructed using the ordered subsets expectation maximization (OSEM) algorithm (two iterations, 21 subsets, no additional filtering). Normalization and corrections were applied for attenuation, scatter, randoms and dead-time. PET/CT hand images were reconstructed so as to have a matrix size of 256 × 256 and a voxel size of 1.199 × 1.199 × 3.27 mm.

Acquisition of PEM images (arthro-PET)

Following dedicated hand PET/CT acquisition, hand PEM imaging was performed on a Naviscan PEM Flex Solo I system (San Diego, CA) (Fig. 1). This is a limited angle tomography system, with two planar detectors of lutetium oxyorthosilicate (LSO) crystals coupled to position-sensitive photomultiplier tubes [31]. The mean FWHM spatial resolutions measured at several locations within the FOV for three different breast compression thicknesses for the PEM Flex Solo II system (very similar to the PEM Flex Solo I system) were found to be 2.4±0.3 mm for in-plane images and 8.0±1.0 mm for cross-plane images [31]. In this study imaging with the PEM system did not involve any extra radiation exposure and the patients did not receive an additional radiopharmaceutical injection. No modification was made to the PEM scanner.

The patients were seated on a chair provided with the PEM system, with the elbow of the imaged hand resting on an adjoining portable support table for patient comfort (see Fig. 1). The patient’s hand was positioned palmar side down on the lower detector so as to entirely include the fingers and wrist joint. The detectors were located in a craniocaudal position. The upper detector was lowered to bring the two detector heads as close together as possible to improve spatial resolution and minimize motion, while providing continuous mild compression of the hand without causing discomfort. A detector separation width between 4.5 and 6 cm was achieved, depending on the individual’s wrist dimensions.

Each PEM hand acquisition involved a 10-min emission scan (24 cm detector sweep) per hand/wrist in a craniocaudal view, followed by another 10-min emission time for the contralateral hand/wrist. Images were reconstructed on the Naviscan workstation, resulting in images with pixels of 1.2 × 1.2 mm and a variable slice thickness dependent on the detector separation of each patient study.

Classification of arthritis

After accrual, patients were classified into two groups: OA or controls, based on a combination of clinical and radiographic findings. The control group included patients with no clinical symptoms or signs of arthritis in the hands based on the ACR OA classification, and no radiographic features of OA [29, 32]. The OA group included patients with clinical signs and symptoms of OA including hard tissue joint enlargement in more than two of ten joints; more than two distal interphalangeal joints (DIPJs); fewer than three swollen metacarpophalangeal joints (MCPJs); or deformity in more than one of ten joints, and radiographic features of OA.

Image analysis/quantitation

PET/CT, arthro-PET and radiography hand images were anonymized. Blinded random order review of each modality by itself was performed by a single radiologist (J.M.) to determine the severity of arthritis after initial scoring consensus with two other radiologists (R.W. and J.C.). Radiographs were scored for the presence and severity of OA using the OARSI scoring method proposed by Altman and Gold [29] with modification.

In each hand 16 joints were assessed (32 joints per patient), with a total of 448 joints scored (Fig. 2). The MCPJs, DIPJs, proximal interphalangeal joints, interphalangeal joint of the thumbs, first carpometacarpal (CMC) joints and scaphotrapeziotrapezoidal joint of the wrists [33] were scored. Radiographic features were graded for the degree of osteophytosis, joint space narrowing, malalignment, presence of central erosions, subchondral sclerosis and subchondral cyst formation (Fig. 2). A sum or total radiographic joint score was determined in each patient.

Region-based quantitative and qualitative metabolic analyses were performed for the arthro-PET and PET/CT images using a four-point scale scoring method (from low to high uptake). Joint uptake was qualitatively classified as *0* less than background, *1* similar to background, *2* greater than background, and *3* substantially greater than background. Spherical regions of interest (ROI) were drawn around each of the joints excluding the skin to quantify the FDG uptake and record the maximum pixel value. The maximum SUV-lean on PET/CT (SUL-Max) was quantified. Similarly for the arthro-PET images, an Xeleris workstation (GE Healthcare, Waukesha, WI) was used to display the apparent SUL values (no attenuation correction was applied to the arthro-PET images). Spherical ROIs were drawn on the arthro-PET hand images to record the maximum pixel values. The total joint glycolytic SUL-Max score from the PET/CT (attenuation-corrected) images and the total maximum pixel values from the arthro-PET images were calculated for each patient by adding the respective data for all 32 joints. Spherical background ROIs were also drawn around each of the mid-aspects of the metacarpal bones in areas devoid of muscle or tissue.

Statistical analysis

Descriptive statistics were calculated. Means were compared using the two-tailed paired Student's *t* test. The gender difference between the OA group and controls was compared using Barnard's exact test. Least squares regression was used to compare the imaging parameters between the two groups adjusting for age and gender. Correlations were assessed by Pearson's correlation coefficient. *P* values <0.05 were considered significant. Data analyses were performed using the statistical software e packages SPSS (SPSS Inc., Chicago, IL) and Excel (Microsoft, Redmond, WA). The described region-based joint scores were subsequently dichotomized whereby 0 and 1 were classified as PET/PEM-negative for joint involvement and scores 2 and 3 were classified as PET/PEM-positive for joint involvement.

Results

Patient characteristics are presented in Table 1 with the OA group comprising eight patients mean age 73±7.7 years) and the control group compromising six patients (53.7±9.3 years). There was no significant difference between the two groups in the baseline blood glucose, injected tracer activity dose, and PET/CT and PEM scan uptake times.

Qualitative arthro-PET summed visual joint scores were significantly higher in the OA group than in controls (38.7±6.6 vs. 32.2±0.4, p =0.02; Table 2). Qualitative PET/CT summed visual joint scores were higher in the OA group than in controls (37.5±5.4 vs. 32.2±0.4, p=0.03; Table 2). Control subjects typically showed little joint activity while OA subjects showed areas of joint activity often, though not invariably, matching the radiographic abnormalities.

Correlation results in the OA group are shown in Fig. 3 and overall showed generally good correlations between and within modalities. The arthro-PET semiquantitative and PET/CT quantitative (SUL-Max) total joint glycolytic scores were highly correlated (r=0.86, p=0.007), as were the arthro-PET and PET/CT qualitative visual joint scores (r =0.94, p=0.001; Fig. 3a). The arthro-PET semiquantitative total joint glycolytic score and the PET/CT quantitative total SUL-Max joint score were higher in the OA group than in the control group (20.8±4.2 vs. 18±1.8, p =0.13; and 22.8±5.38 vs. 20.1±1.54, p = 0.21, respectively). The arthro-PET qualitative and semiquantitative total joint scores were correlated (r =0.82, p =0.01), as was the PET/CT visual joint score and the PET/CT quantitative score (p=0.01; Fig. 3b). The radiographic score was positively correlated with the arthro-PET semiquantitative total glycolytic joint score (r =0.73, p=0.04) and the total PET/CT SUL-Max joint score (r=0.67, p =0.07; Fig. 3c). By definition, the OA group had a higher quantitative total radiographic joint score than the control group (30.9±31.3 vs. 0, p=0.03).

Example images in control and OA patients are shown in Figs. 4 and 5.

Discussion

This prospective pilot study demonstrated that small joint imaging using an ^{18}F-FDG PEM system (arthro-PET) is feasible for hand OA evaluation. Arthro-PET performed comparably to PET/CT with both using a dedicated high-resolution imaging protocol. Quantitative and qualitative visual metabolic activity corresponded with radiographically evident and clinically symptomatic OA, discriminating these patients from controls.We found significant correlations between the arthro-PET and PET/CT qualitative and quantitative scores in the OA group. The qualitative total arthro-PET and PET/CT visual joint scores were significantly higher in the OA group than in the control group. The quantitative summed arthro-PET and PET/CT scores were also higher in the OA group, but did not reach statistical significance.

Our choice of OA imaging was to ensure the feasibility of the imaging method while comparing it with a known metabolic standard (PET/CT). Several previous studies using WB PET/CT have demonstrated increased FDG uptake in rheumatoid arthritis, erosive joint arthritis and OA, correlating with metabolic and clinical parameters and synovial joint volume on MRI, which supports the use of FDG PET in arthritis [16, 17, 20–26]. OA is also the most common form of arthritis. Although we describe the method in patients with OA, this group of patients may not benefit the most in the future when compared to patients with other inflammatory arthritides such as rheumatoid arthritis for which disease-modifying therapy exists.

The classification of hand OA is complex and often multi-factorial, and is compounded by the fact that the hand is a small non-weight-bearing structure. The pathophysiology of OA involves changes in articular cartilage, subchondral bone and synovium, all three tissues of which undergo alterations in concert at the structural levels in response to mechanical stress and joint malalignment [34, 35]. OA is also further morphologically classified into a nodal form and an erosive form [35]. Different imaging modalities may be better suited to evaluating a different stage of the disease process.

We imaged the hand joints in patients initially referred for an oncologically oriented FDG PET scan, some of whom had radiographic OA joint changes. Although radiographs are typically used to diagnose OA, they have not been proven to be the gold standard, and tend to demonstrate advanced OA findings in subchondral bone, with joint space loss and misalignment. MRI is able to depict the early changes in articular cartilage degeneration and ligamentous integrity, and may show bone marrow lesions and synovitis that may correlate with clinical symptoms [35]. Differentiating active (and thus potentially reversible) disease versus irreversible damage in OA is vital, as it enables the use of targeted therapy to reverse inflammation [36]. MRI imaging including gadolinium contrast enhancement may further depict structural changes in the joint as well as synovial inflammation. FDG PET can demonstrate the degree of joint inflammation following release of proinflammatory cytokines and inflammatory mediators in active arthritis.

The criteria for OA based on anatomy are clearly defined, but the anatomical controls may not be appropriate for the inflammatory component of OA, as some joints may be

anatomically altered but metabolically quiescent. Several disparities exist between anatomical OA and the metabolic (inflammatory) phenotypes as shown in this study, likely owing to the different stages of disease being depicted. Of note, not all radiographic foci of OA in our study were FDG-avid, indicating that while correlated with anatomical imaging, the arthro-PET and radiographic findings were not identical, suggesting an added value of functional over morphological imaging. Our description of PEM (arthro-PET) imaging may be of interest as there is increasing awareness that inflammation may precede joint destruction in OA, and may facilitate the damage to the underlying joint.

Radiolabeled bisphosphonates (^{99m}Tc-MDP) with planar and SPECT/CT bone scanning have also demonstrated OA disease activity in both the early and late phases of disease in nodal OA when compared to radiography alone [37, 38]. ^{99m}Tc-MDP uptake is a very sensitive but often a nonspecific tool for visualizing bone metabolism, often accumulating in fractures, inflammation, infection and degenerative disease, for example, and it is not clear which pathological process of OA is depicted by ^{99m}Tc-MDP [37]. Although SPECT/CT has superior spatial resolution to planar bone scintigraphy with higher lesion detection rates [38], the spatial resolution of PET/CT (and PEM/arthro-PET) is far superior to both. ^{18}F-NaF PET/CT has also proved useful in assessing suspected painful large-joint OA in the human knee [39]. ^{18}F-NaF is selectively incorporated into bone at sites of bone remodeling due to the activity of osteoblasts and osteoclasts, and offers better spatial resolution than ^{99m}Tc-MDP. Its role in imaging hand OA has not been investigated to our knowledge. The use of bone metabolic imaging should thus be carefully tailored to the clinical scenario. Due to its mechanism of uptake, ^{18}F-FDG currently appears more specific for inflammation imaging and may be better able to depict the inflammatory component in hand OA rather than radiolabeled bisphosphonates and ^{18}F-NaF which may instead be better tailored to depicting subchondral changes related to bone turnover.

This study was a feasibility study to assess the role of PEM imaging systems in hand OA, a common arthropathy affecting a large proportion of the population. In a previous study a different dedicated small-parts breast PET/CT imaging system (which consisted of an LSO-based dual-planar head PET camera and a cone-beam CT system, where the patient lay prone on a specialized bed and inserted the hand through an aperture in the table top) was used to image a patient with rheumatoid arthritis and associated OA [40, 41]. The imaging system we used was FDA-cleared, simpler and widely disseminated. We chose prone positioning with extended arms for the extremity PET/CT component in our study to avoid scatter or loss of counts, which would have occurred if the hands had been placed on the abdomen. A future study may also involve imaging at multiple time points to determine the optimal imaging time. A lower injected radiotracer dose could potentially be administered for dedicated extremity joint imaging, thereby improving dosimetry. With the FOV of the current PEM system, the wrist might not be fully included in a larger patient in one acquisition, but the wrist could be scanned separately.

“Increased” FDG activity was noted at the skin edge on PEM, similar to non-attenuation-corrected PET/CT images. This was a nonspecific finding and was seen in all patients including the controls. This did not appear to affect the qualitative assessment of the joints, as diseased joints had significantly higher uptake compared to background skin uptake.

When placing ROIs for quantitation, the reader must be aware of these normal patterns of uptake on arthro-PET, which are similar to those seen on non-attenuation-corrected PET images. It is possible that skin uptake values may be variable. We did not encounter any issues with patient motion artifacts. Patients likely should be counseled to avoid exercise prior to PEM or PET imaging in order to avoid increased physiological hand muscle uptake, which may partly obscure the thumb CMC joint.

Dedicated PEM systems based upon limited-angle tomography have high spatial resolution in planes parallel to the detectors but much poorer resolution in the direction between the detectors. Lodge et al. have previously characterized the effect of this asymmetry on the contrast observed in experimetal phantom images using the Naviscan PEM Flex Solo I system [42]. Between-plane resolution degrades as detector separation increases, so this PEM design is well-suited to hand imaging where the detector separation is only 4.5 – 6 cm. Springer et al. determined that applying corrections for count rate, attenuation and scatter was essential for the PEM Flex Solo II system, with the least attenuation effects seen in phantoms of thickness 4 cm [43]. A dedicated small-parts system like PEM has high spatial resolution, and in breast applications, has been shown to have comparable sensitivity and specificity to MRI for breast lesions [44]. The small PEM detector separation reduces resolution loss due to annihilation photon noncolinearity [28]. Breast-only devices suffer from much less attenuation loss than WB scanners, with up to a tenfold increase in count efficiency [41]. The lack of attenuation correction in the PEM device, unlike with WB PET/CT, complicates absolute quantitation. However, there is limited soft tissue attenuation in the hand and a PEM uptake value could still be calculated. An advantage of PET/CT is the anatomical correlate with low-dose CT, possibly obviating the need for radiographs, but the hand positioning with PEM is easier in patients, and can be done in a separate room dedicated to PEM, while freeing up the PET/CT scanner for routine WB studies.

Arthro-PET was able to depict joint metabolic activity with quality similar to that with an optimized high-resolution PET/CT protocol. The advantages of arthro-PET over WB PET/CT include image acquisition while the patient is sitting upright with more comfort for patients unable to lie prone. Arthro-PET provides simpler positional requirements than other PET/CT devices designed to image small body parts [34] where the patient must be prone. The smaller PEM device is portable and could be placed in an adequately shielded imaging room, is much less costly than WB PET/CT, and produces comparable performance. Arthro-PET may be a suitable alternative in patients in whom MR imaging or administration of intravenous gadolinium-based contrast agents (required to assess synovial inflammation) are contraindicated, or in patients who suffer from significant claustrophobia.

The limitations of this study include the small number of patients, lack of correlation with other modalities (MRI, ultrasonography) and absence of a treatment group. The results of this study, however, should be viewed within the context of the study design. It should be emphasized that our group of patients had been referred for an oncologically oriented FDG PET scan, and that their OA was most likely a coincidental condition linked to advanced age, and we were therefore limited to determining OA disease activity at the time of the scans. The small sample size reduced our ability to make inferences and may explain the lack of statistically significant differences for some quantitative values. Additional studies

with a larger sample size are needed to improve the statistical power, and refine interpretation criteria. The calculation of an appropriate sample size could be based on our pilot data since it is currently unclear which quantitative metric is most appropriate in assessing arthritis activity.

Unlike inflammatory arthritides such as rheumatoid arthritis in which pain and/or disability are constant, only 15 % of patients exhibiting radiographic OA of the hands report pain, with a modest to weak correlation between radiographic OA and clinical symptoms such as pain and/or disability [45]. Thus, we advise using caution in extrapolating the study findings from this limited-sized cohort of patients. Comparison with other advanced imaging modalities such as MRI and ultrasonography would provide an insight into whether arthro-PET activity corresponds to synovitis and/or marrow lesions. PET may more precisely define the volume of metabolically active synovium, which is difficult with other modalities. Major potential advantages may lie in the ability¿ to quantitatively assess disease activity before and after treatment, thereby potentially acting as an imaging biomarker, contributing to patient management. Arthro-PET methods could potentially be eventually expanded for inclusion in trials in classic inflammatory arthritides where arthro-PET may have a greater role in rheumatoid arthritis and psoriatic arthritis, as the pathogenesis and therapy of these conditions are more clearly inflammatory. A study exploring the performance of the PEM system in monitoring the efficacy of treatment would provide further meaningful information. A treatment group would allow estimation of sensitivity to change, an important feature for biomarkers and potential for prognostic information to determine which patients are more likely to show a therapeutic effect. The exact clinical role of arthro-PET in the evaluation of OA needs to be determined prospectively in larger cohorts.

Finally, the principles of the OMERACT process aimed at improving outcome measurements in rheumatology which have already been applied to MRI [44], will also likely need to be applied to FDG PET imaging in arthritis, in order to determine which indices (e.g. visual metabolic score versus quantitative SUV) and outcome measurements will allow comparison across studies in future trials.

In summary, FDG arthro-PET hand imaging is feasible, performing comparably to dedicated PET/CT in discriminating OA from non-OA patients. Further exploration of FDG arthro-PET is warranted in larger cohorts of arthritis patients.

References

1. Hayashi D, Roemer FW, Guermazi A. Osteoarthritis year 2011 in review: imaging in OA – a radiologists' perspective. Osteoarthritis Cartilage. 2012; 20:207–214. [PubMed: 22266236]
2. Sofat N, Ejindu V, Kiely P. What makes osteoarthritis painful? The evidence for local and central pain processing. Rheumatology (Oxford). 2011; 50:2157–2165. [PubMed: 21954151]
3. Guermazi A, Hayashi D, Eckstein F, Hunter DJ, Duryea J, Roemer FW. Imaging of osteoarthritis. Rheum Dis Clin N Am. 2013; 39:67–105.
4. Dahaghin S, Bierma-Zeinstra SM, Ginai AZ, Pols HA, Hazes JM, Koes BW. Prevalence and pattern of radiographic hand osteoarthritis and association with pain and disability (the Rotterdam study). Ann Rheum Dis. 2005; 64:682–687. [PubMed: 15374852]

5. Hayashi D, Roemer FW, Katur A, Felson DT, Yang SO, Alomran F, Guermazi A. Imaging of synovitis in osteoarthritis: current status and outlook. Semin Arthritis Rheum. 2011; 41:116–130. [PubMed: 21295331]

6. Beltran J, Chandnani V, McGhee RA Jr, Kursunoglu-Brahme S. Gadopentetate dimeglumine-enhanced MR imaging of the musculoskeletal system. AJR Am J Roentgenol. 1991; 156:457–466. [PubMed: 1899738]

7. Iagnocco A, Perella C, D'Agostino MA, Sabatini E, Valesini G, Conaghan PG. Magnetic resonance and ultrasonography real-time fusion imaging of the hand and wrist in osteoarthritis and rheumatoid arthritis. Rheumatology (Oxford). 2011; 50:1409–1413. [PubMed: 21406468]

8. Keen HI, Mease PJ, Bingham CO 3rd, Giles JT, Kaeley G, Conaghan PG. Systematic review of MRI, ultrasound, and scintigraphy as outcome measures for structural pathology in interventional therapeutic studies of knee arthritis: focus on responsiveness. J Rheumatol. 2011; 38:142–154. [PubMed: 20889598]

9. Omoumi P, Mercier GA, Lecouvet F, Simoni P, Vande Berg BC. CT arthrography, MR arthrography, PET, and scintigraphy in osteoarthritis. Radiol Clin N Am. 2009; 47:595–615. [PubMed: 19631071]

10. Biswal S, Resnick DL, Hoffman JM, Gambhir SS. Molecular imaging: integration of molecular imaging into the musculoskeletal imaging practice. Radiology. 2007; 244:651–671. [PubMed: 17709823]

11. Maurer AH, Holder LE, Espinola DA, Rupani HD, Wilgis EF. Three-phase radionuclide scintigraphy of the hand. Radiology. 1983; 146:761–775. [PubMed: 6219422]

12. Backhaus M, Kamradt T, Sandrock D, Loreck D, Fritz J, Wolf KJ, et al. Arthritis of the finger joints: a comprehensive approach comparing conventional radiography, scintigraphy, ultrasound, and contrast-enhanced magnetic resonance imaging. Arthritis Rheum. 1999; 42:1232–1245. [PubMed: 10366117]

13. Umemoto Y, Oka T, Inoue T, Saito T. Imaging of a rat osteoarthritis model using (18)F-fluoride positron emission tomography. Ann Nucl Med. 2010; 24:663–669. [PubMed: 20809138]

14. Hashefi M, Curiel R. Future and upcoming non-neoplastic applications of PET/CT imaging. Ann N YAcad Sci. 2011; 1228:167–174.

15. Shreve PD, Anzai Y, Wahl RL. Pitfalls in oncologic diagnosis with FDG PET imaging: physiologic and benign variants. Radiographics. 1999; 19:61–77. [PubMed: 9925392]

16. Elzinga EH, van der Laken CJ, Comans EF, Lammertsma AA, Dijkmans BA, Voskuyl AE. 2-Deoxy-2-[F-18]fluoro-D-glucose joint uptake on positron emission tomography images: rheumatoid arthritis versus osteoarthritis. Mol Imaging Biol. 2007; 9:357–360. [PubMed: 17902022]

17. Beckers C, Ribbens C, Andre B, Marcelis S, Kaye O, Mathy L, et al. Assessment of disease activity in rheumatoid arthritis with (18)F-FDG PET. J Nucl Med. 2004; 45:956–964. [PubMed: 15181130]

18. Goerres GW, Forster A, Uebelhart D, Seifert B, Treyer V, Michel B, et al. F-18 FDG whole-body PET for the assessment of disease activity in patients with rheumatoid arthritis. Clin Nucl Med. 2006; 31:386–390. [PubMed: 16785804]

19. Miese F, Scherer A, Ostendorf B, Heinzel A, Lanzman RS, Kröpil P, et al. Hybrid 18F-FDG PET-MRI of the hand in rheumatoid arthritis: initial results. Clin Rheumatol. 2011; 30:1247–1250. [PubMed: 21590292]

20. Polisson RP, Schoenberg OI, Fischman A, Rubin R, Simon LS, Rosenthal D, et al. Use of magnetic resonance imaging and positron emission tomography in the assessment of synovial volume and glucosemetabolism in patients with rheumatoid arthritis. Arthritis Rheum. 1995; 38:819–825. [PubMed: 7779126]

21. Beckers C, Jeukens X, Ribbens C, André B, Marcelis S, Leclercq P, et al. (18)F-FDG PET imaging of rheumatoid knee synovitis correlates with dynamic magnetic resonance and sonographic assessments as well as with the serum level of metalloproteinase-3. Eur J Nucl Med Mol Imaging. 2006; 33:275–280. [PubMed: 16247604]

22. Nakamura H, Masuko K, Yudoh K, Kato T, Nishioka K, Sugihara T, et al. Positron emission tomography with 18F-FDG in osteoarthritic knee. Osteoarthritis Cartilage. 2007; 15:673–681. [PubMed: 17336549]
23. Rosen RS, Fayad L, Wahl RL. Increased 18F-FDG uptake in degenerative disease of the spine: characterization with 18F-FDG PET/CT. J Nucl Med. 2006; 47:1274–1280. [PubMed: 16883005]
24. Palmer WE, Rosenthal DI, Schoenberg OI, Fischman AJ, Simon LS, Rubin RH, et al. Quantification of inflammation in the wrist with gadolinium-enhanced MR imaging and PET with 2-[F-18]-fluoro-2-deoxy-D-glucose. Radiology. 1995; 196:647–655. [PubMed: 7644624]
25. Houseni M, Chamroonrat W, Zhuang H, Alavi A. Facet joint arthropathy demonstrated on FDG-PET. Clin Nucl Med. 2006; 31:418–419. [PubMed: 16785814]
26. Wandler E, Kramer EL, Sherman O, Babb J, Scarola J, Rafii M. Diffuse FDG shoulder uptake on PET is associated with clinical findings of osteoarthritis. AJR Am J Roentgenol. 2005; 185:797–803. [PubMed: 16120937]
27. Liu Y, Ghesani NV, Zuckier LS. Physiology and pathophysiology of incidental findings detected on FDG-PET scintigraphy. Semin Nucl Med. 2010; 40:294–315. [PubMed: 20513451]
28. Weinberg IN. Applications for positron emission mammography. Phys Med. 2006; 21:132–137. [PubMed: 17646015]
29. Altman RD, Gold GE. Atlas of individual radiographic features in osteoarthritis, revised. Osteoarthritis Cartilage. 2007; 15:1–56. [PubMed: 16891130]
30. Lodge MA, Chaudhry MA, Udall DN, Wahl RL. Characterization of a perirectal artifact in 18F-FDG PET/CT. J Nucl Med. 2010; 51:1501–1506. [PubMed: 20847169]
31. MacDonald L, Edwards J, Lewellen T, Haseley D, Rogers J, Kinahan P. Clinical imaging characteristics of the positron emission mammography camera: PEM Flex Solo II. J Nucl Med. 2009; 50:1666–1675. [PubMed: 19759118]
32. Kellgren JH, Lawrence JS. Radiological assessment of osteoarthrosis. Ann Rheum Dis. 1957; 16:494–502. [PubMed: 13498604]
33. Wollstein R, Clavijo J, Gilula LA. Osteoarthritis of the wrist STT joint and radiocarpal joint. Arthritis. 2012; 2012:242159. [PubMed: 22957252]
34. Samuels J, Krasnokutsky S, Abramson SB. Osteoarthritis: a tale of three tissues. Bull NYU Hosp Jt Dis. 2008; 66(3):244–250. [PubMed: 18937640]
35. McGonagle D, Tan AL, Carey J, Benjamin M. The anatomical basis for a novel classification of osteoarthritis and allied disorders. J Anat. 2010; 216(3):279–291. [PubMed: 20070426]
36. Guillemin F. How to assess musculoskeletal conditions. Assessment of disease activity. Best Pract Res Clin Rheumatol. 2003; 17(3):415–426. [PubMed: 12787510]
37. Hutton CW, Higgs ER, Jackson PC, Watt I, Dieppe PA. 99mTc HMDP bone scanning in generalised nodal osteoarthritis. II. The four hour bone scan image predicts radiographic change. Ann Rheum Dis. 1986; 45(8):622–626. [PubMed: 3740991]
38. Schleich FS, Schürch M, Huellner MW, Hug U, von Wartburg U, Strobel K, Veit-Haibach P. Diagnostic and therapeutic impact of SPECT/CT in patients with unspecific pain of the hand and wrist. EJNMMI Res. 2012; 2(1):53. [PubMed: 23021154]
39. Draper CE, Quon A, Fredericson M, Besier TF, Delp SL, Beaupre GS, Gold GE. Comparison of MRI and ^{1} F-NaF PET/CT in patients with patellofemoral pain. J Magn Reson Imaging. 2012; 36(4):928–932. [PubMed: 22549985]
40. Bowen SL, Wu Y, Chaudhari AJ, et al. Initial characterization of a dedicated breast PET/CT scanner during human imaging. J Nucl Med. 2009; 50:1401–1408. [PubMed: 19690029]
41. Chaudhari AJ, Bowen SL, Burkett GW, et al. High-resolution (18)F-FDG PET with MRI for monitoring response to treatment in rheumatoid arthritis. Eur J Nucl Med Mol Imaging. 2010; 37:1047. [PubMed: 20119695]
42. Lodge M. JNM, Meeting Abstracts. 2011; 52:433.
43. Springer A, Mawlawi OR. Evaluation of the quantitative accuracy of a commercially available positronemission mammography scanner. Med. Phys. 2011; 38(4):2132–2139. [PubMed: 21626946]

44. Narayanan D, Madsen KS, Kalinyak JE, Berg WA. Interpretation of positron emission mammography and MRI by experienced breast imaging radiologists: performance and observer reproducibility. AJR Am J Roentgenol. 2011; 196:971–981. [PubMed: 21427351]

45. Tugwell P, Boers M, Brooks P, Simon L, Strand V, Idzerda L. OMERACT: An international initiative to improve outcome measurement in rheumatology. Trials. 2007; 8:38. [PubMed: 18039364]

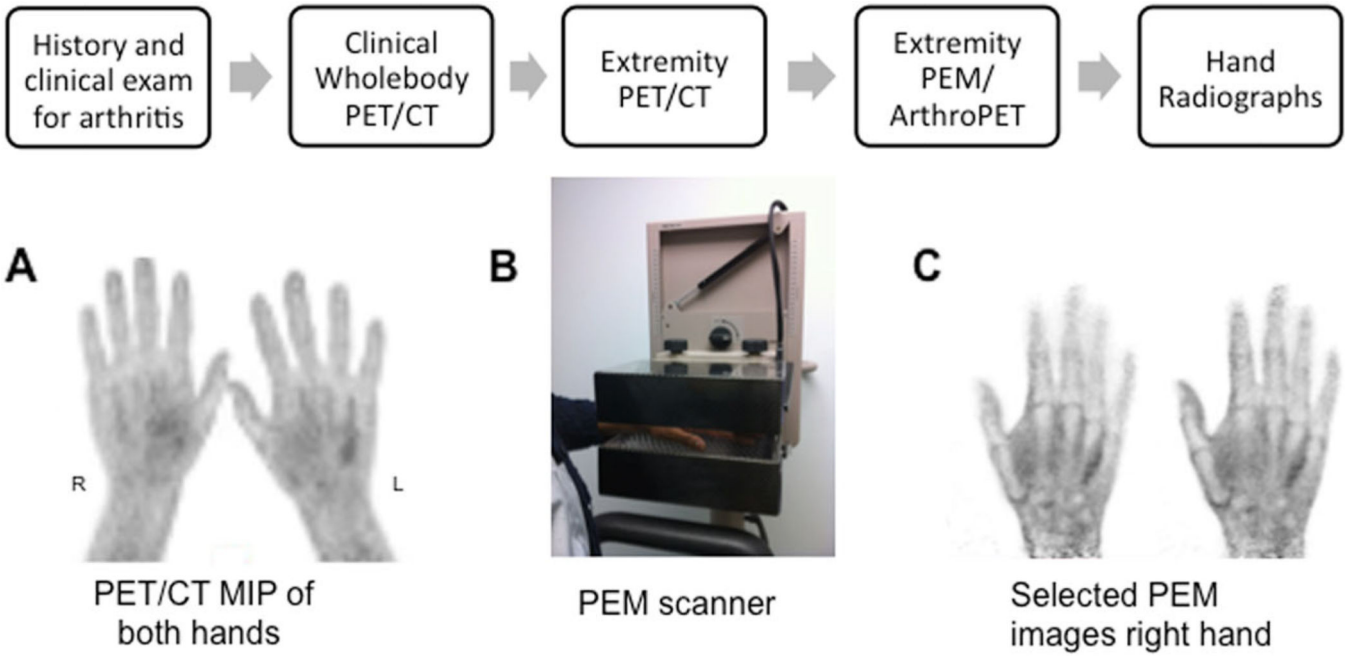

Fig. 1.

Imaging sequence protocol. Following WB PET/CT, dedicated PET/CT of the hands was performed with the patient lying prone (**a**). PEM imaging of each hand was performed using a Naviscan PEM Flex Solo I system (**b, c**). The hand was positioned palmar side down on the lower detector head (**b**). Selected PEM hand images are shown in (**c**). *MIP* maximum intensity projection image, *PEM* positron emission mammography

	SCORE	JOINTS
Osteophytes	0-3	(DIP,PIP,CMC1)
	0-1	(IPJ1,STT)
Joint Space Narrowing	0-3	(DIP,PIP,CMC1)
	0-1	(IPJ1,STT)
Malalignment	0-1	(DIP,PIP,CMC1)
Erosions	0-1	DIP (central, pseudo-widening);PIP,CMC1
Subchondral sclerosis	0-1	(DIP,PIP,CMC1)
Subchondral cysts	0-1	(PIP,CMC1)

Fig. 2.

Radiographic joint scoring: 16 joints were assessed per hand (32 joints per patient). Individual radiographic features were scored per joint for the severity of OA as normal, and 1+, 2+ and 3+ change (blinded to both the PET and arthro-PET images) using the Altman radiographic scoring method, and the total radiographic joint score was calculated. *IPJ* interphalangeal joint (*D* distal, *P* proximal), *CMC* carpometacarpal joint, *STT* scaphotrapeziotrapezoidal joint

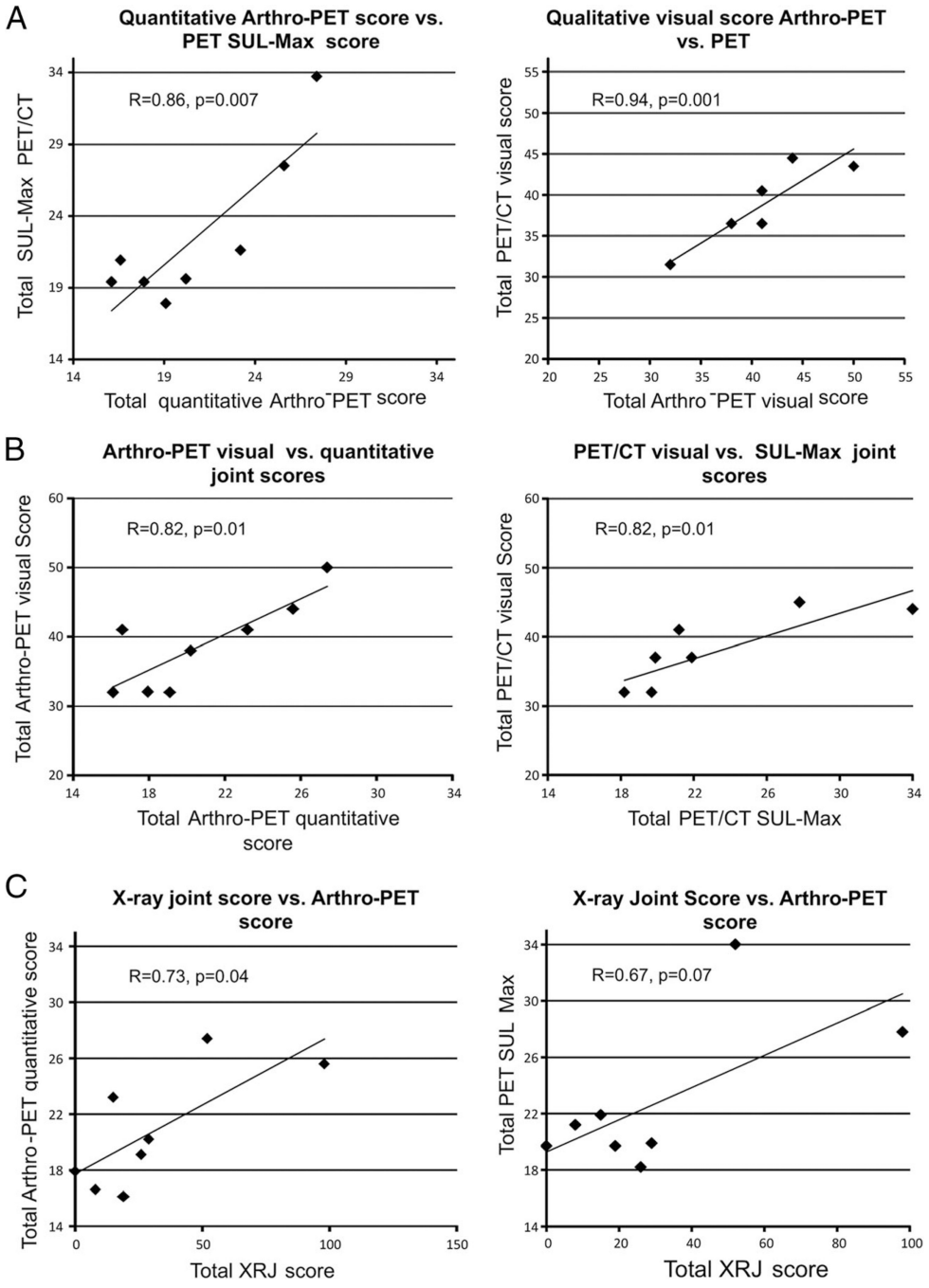

Fig. 3.

Correlations between joint scores in OA patients. **a** Total arthro-PET vs. PET/CT glycolytic scores. **b** Qualitative visual vs. quantitative SUL-Max scores. **c** Total radiographic (*XRJ*) vs. total glycolytic scores

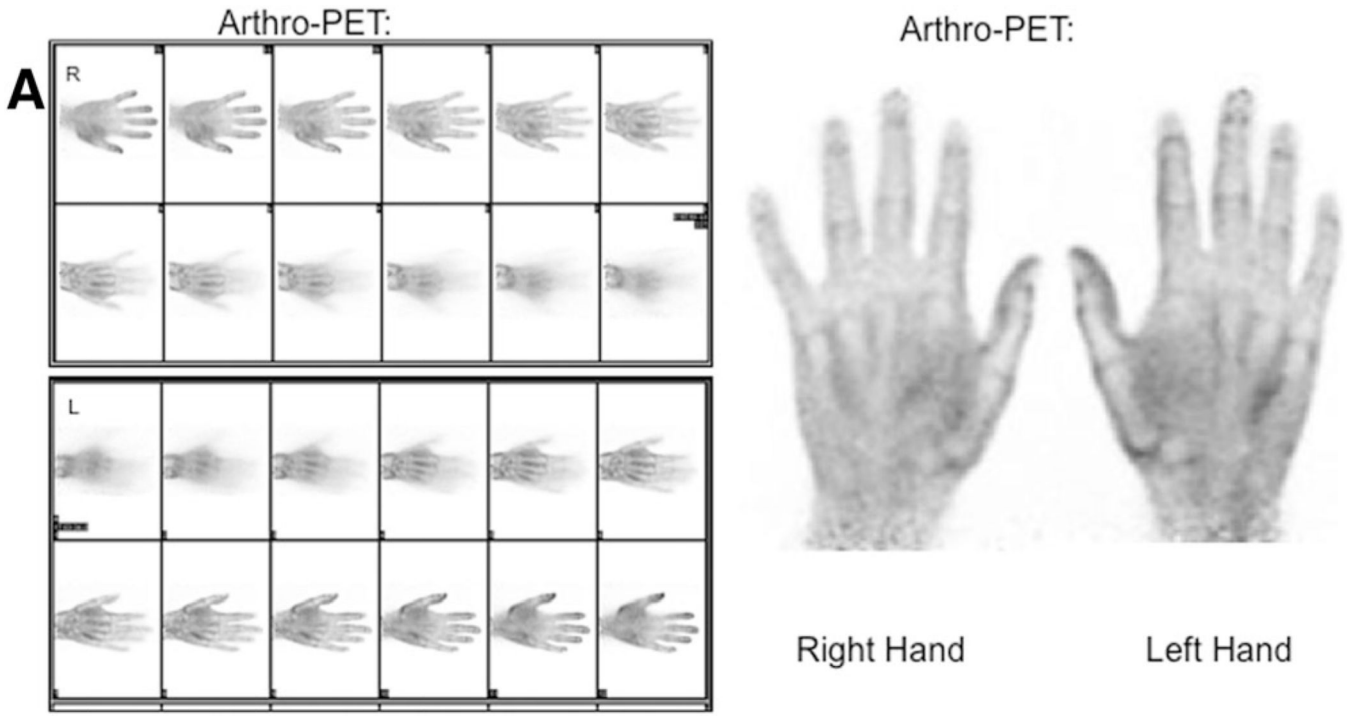

Fig. 4.

^{18}F-FDG arthro-PET images in a 48-year-old asymptomatic (control) male patient without radiographic changes. The PEM scanner produces 12 individual frames per hand during the 10 min of imaging (**a**)

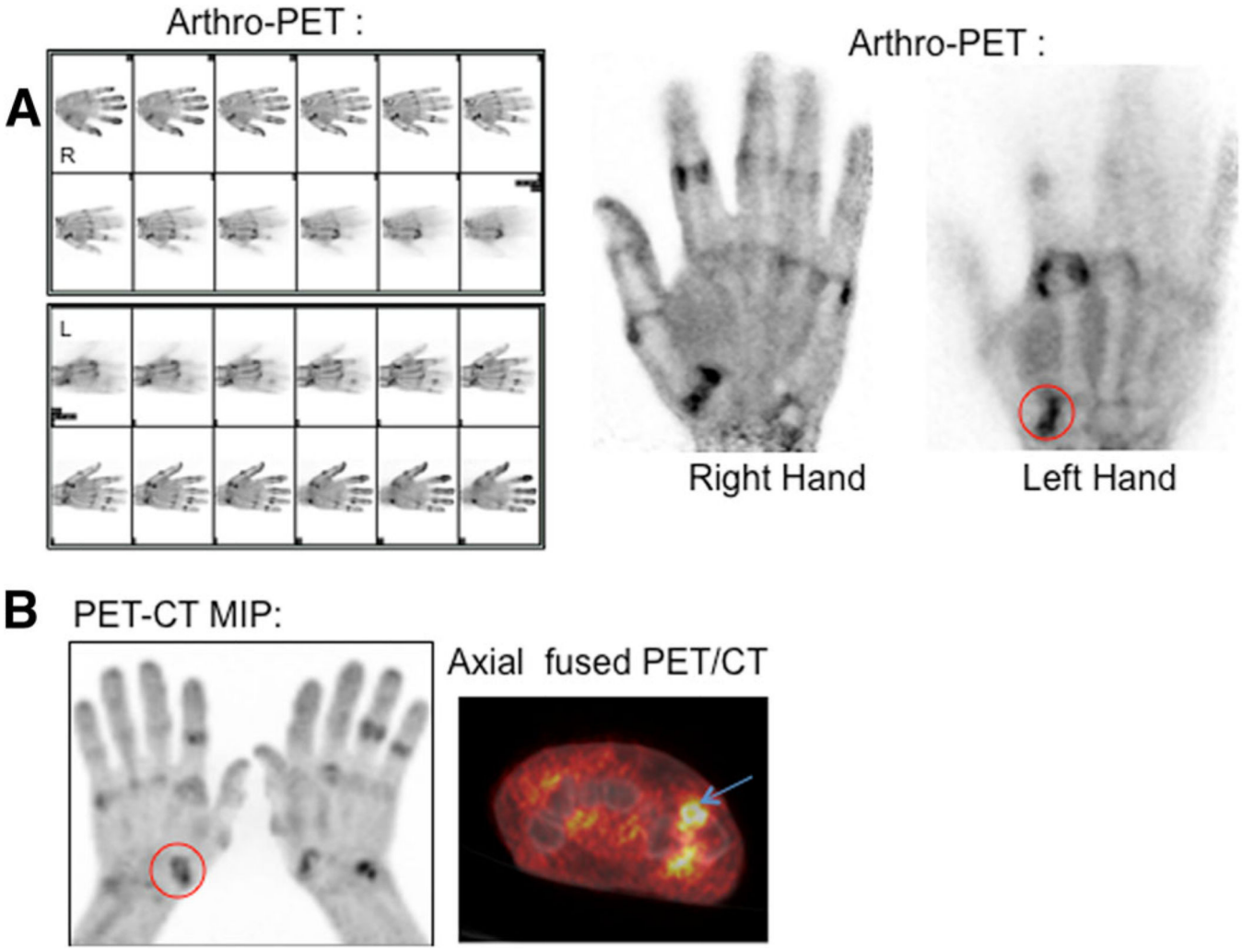

Fig. 5.

^{18}F-FDG imaging in a 70-year-old symptomatic male patient with radiographic evidence of erosive OA: **a** arthro-PET images and **b** PET/CT maximum intensity projection images show hypermetabolic OA. A representative OA joint, the left first CMC joint (*circles*), is shown on the arthro-PET image (**a**) and PET/CT image (**b**). The PEM scanner produces 12 individual frames per hand during the 10 min of imaging (**a**)

Table 1

Patient characteristics

Characteristic	Group			*P* value
	All	OA (*n*=8)	Controls (*n*=6)	
Age (years), mean ± SD (range)	64.7±12.8	73±7.71 (65 – 85)	53.7±9.3 (41 – 68)	0.001
Gender, *n* (%)				
Female	7 (50)	5 (62.5)	2 (33.3)	0.45
Male	7 (50)	3 (37.5)	4 (66.7)	
Blood glucose (mg/dL), mean ± SD		104.9±22	99.7±8.23	0.55
Injected FDG dose (mCi), mean ± SD		16.3±4.30	16.1±2.87	0.91
Uptake time (min), mean ± SD				
WB PET		62.1±6.75	57.3±3.72	0.11
Arthro-PET		130.9±13.3	133.5±13.4	0.72

Table 2

Joint score results

Score	Group		*P* value
	OA (*n*=8)	Controls (*n*=6)	
Arthro-PET sum qualitative visual joint score	38.75±6.56	32.17±0.41	0.025
PET/CT sum qualitative visual joint score	37.5±5.37	32.17±0.41	0.029
Arthro-PET quantitative total joint glycolytic score	20.8±4.2	18±1.8	0.13
PET quantitative total joint glycolytic score	22.8±5.4	20.1±1.5	0.21
Radiographic quantitative total joint score	30.9±31.3	0	0.03

The data are presented as ?means±SD